J Mater Sci (2008) 43:5734–5746
DOI 10.1007/s10853-008-2896-3

Effect of electromagnetic stirring on melt pool free surface dynamics during vacuum arc remelting

P. Chapelle · A. Jardy · J. P. Bellot · M. Minvielle

Received: 25 February 2008 / Accepted: 22 July 2008 / Published online: 9 August 2008

Abstract The deformation of the free surface of the liquid pool in the VAR process may play a key role in explaining the apparition of surface defects on the ingot skin. In the present study, the deformation of the surface induced by electromagnetic stirring is investigated, for a simplified geometry, using CFD-based simulations, combining models for the turbulent fluid flow, heat transfer, free surface movements and electromagnetic forces. Particular attention is given to the implementation of thermal and electrical boundary conditions at the moving free surface. Verification of the developed model is carried out by comparison with the dedicated code SOLAR. The free surface dynamics of a liquid zirconium pool is then quantitatively analysed for different stirring procedures, and the effects of the stirring parameters (magnetic induction, reversal time) are predicted and discussed. The obtained results provide some insights into mechanisms by which surface deformation may influence the ingot skin solidification, leading to poor ingot surface quality.

Introduction

The vacuum arc remelting (VAR) process consists in melting under vacuum a consumable electrode by means of an electric arc, with the aim of producing an ingot with improved chemical homogeneity and reduced impurity content. This process is used for industrial manufacturing of reactive metals (titanium and zirconium), nickel-base alloys and special steels. In operation, a DC electric arc, which produces the high temperature needed to melt the electrode, is struck between the tip of the consumable electrode and the secondary ingot (Fig. 1). Liquid metal drops are formed at the electrode tip, and then transferred by gravity to the liquid pool at the top of the ingot. The ingot solidifies in contact with the walls of a water-cooled copper crucible. The furnace is equipped with an external horizontal coil around the crucible, which creates a vertical magnetic field. Electromagnetic stirring induced by the interaction of the magnetic field with the melting current is used, among others, to promote homogenization of the metal in the liquid pool.

Over the past two decades, considerable progress in the understanding of the VAR process has been made by using numerical modelling. Particularly noteworthy contributions to this field are presented in [1–4]. Among those contributions, the numerical code SOLAR developed at the School of Mines in Nancy, which simulates ingot growth and solidification, has proven to be an efficient and valuable tool for the prediction of parameter changes and their impact on the product quality and process efficiency [3, 5, 6]. In this model, the free surface of the liquid pool is considered to be flat and undeformable. Although this approach is able to adequately represent electrical and thermal interactions between the arc plasma and the liquid metal, it does not take into account the free surface dynamics. Indeed, the pool surface is deformed due to the action of electromagnetic stirring, impingement of metal droplets from the consumable electrode, the pressure force produced by the plasma and recoil pressure effects

P. Chapelle (✉) · A. Jardy · J. P. Bellot
Laboratoire de Science et Génie des Matériaux et de Métallurgie (UMR CNRS 7584) Ecole des Mines, Parc de Saurupt, 54042 Nancy cedex, France
e-mail: chapelle@mines.inpl-nancy.fr

M. Minvielle
AREVA, Centre de Recherches de la Compagnie Européenne du Zirconium CEZUS, 73403 Ugine cedex, France

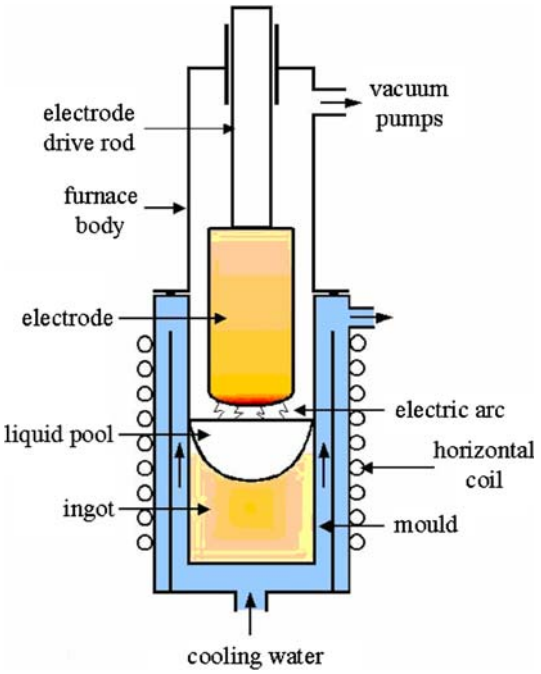

Fig. 1 Schematic principle of the VAR process

associated to metal vaporization at the surface. The magnitude of each of these deformations and the influence of free surface movements on the solidification conditions of the metal, hence the final quality of the ingot, remain poorly understood in the context of the VAR process.

The deformation of the free surface of a liquid metal bath has been extensively investigated in the case of continuous casting of steel, for which it was shown that the final aspect of the ingot surface is very sensitive to this phenomenon. Indeed, the transient evolution of the shape of the free surface may disturb solidification of the first ingot skin in contact with the crucible wall and lead to the apparition of surface defects (like surface depressions or transverse cracks) [7–9]. For example, during sudden variations of the liquid level in the crucible (due to the jet injection of fresh steel), the ingot skin undergoes important thermal stresses, which may cause skin distortion resulting in the formation of a depression on the lateral surface of the ingot [7]. Several studies have shown that the probability of formation of surface defects is significantly decreased by reducing metal liquid level fluctuations in the crucible [9–11]. Obviously, these results cannot be directly transposed to the case of the VAR process. However, they highlight the possible negative effects of liquid metal fluctuations on the ingot surface quality. Hence, accurate prediction of the free surface deformation could be a crucial step in understanding the formation of some defects.

As mentioned above, the deformation of the free surface of the liquid pool in VAR results from several phenomena. In the present paper, we focus our attention on the effect of electromagnetic stirring. The aim of this study is to quantify the deformation of the free surface caused by electromagnetic forces and characterize the dynamic behaviour of the surface, in order to analyse the impact of this deformation on the solidification conditions of the first skin of the ingot. One considers a simplified configuration, consisting of a cylindrical bath of liquid metal, through which a DC electric current is flowing. The bath is submitted to an axial external magnetic field. Liquid metal flow and heat transfer in the bath, as well as the deformation of the top surface, are simulated using the commercial code Fluent v6.2. The paper is organized as follows. In section "Model Description", we present the mathematical model. Section "Model Verification" is concerned with verifications of the model developed. Finally, a series of applications of the model to investigate free surface behaviour during various modes of electromagnetic stirring is presented in section "Results and Discussion".

Model description

Figure 2 shows a schematic sketch of the investigated configuration, which is representative of a liquid pool in a VAR ingot. It consists of a cylindrical crucible containing a liquid metal bath, through which a DC electric current is flowing. The crucible is surrounded by an electromagnetic coil, which produces an external magnetic field across the liquid metal. The calculation method of the deformation of the liquid metal free surface used in this study (see section "Calculation of the Free Surface Deformation") requires to introduce an additional calculation domain above the bath, which is assumed to be filled with air. Note that owing to the high density ratio between the liquid metal and air, the stress produced by the air on the metal surface is negligible. Thus, the present results will not be modified in the

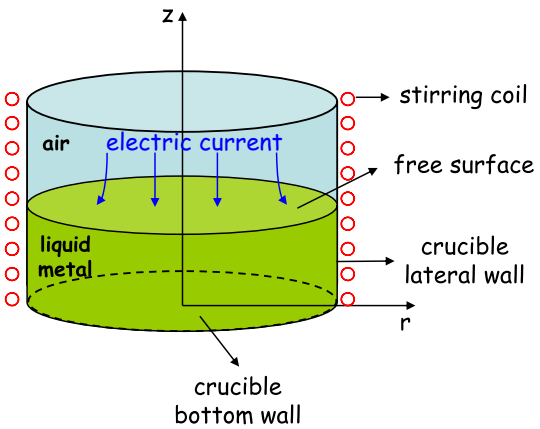

Fig. 2 Geometry of the investigated configuration

presence of vacuum (like in the VAR process) instead of air above the bath.

The model is based on the following assumptions.

- The distribution of temperature and electric current density at the top surface of the bath is considered to be uniform.
- The temperature of the bottom and lateral walls of the crucible is uniform and equal to the liquidus temperature of the metal, which avoids the description of solidification phenomena.
- Perfect electrical contact between the liquid metal and crucible walls is considered.
- Joule heating of liquid metal remains negligible [12].
- The influence of surface tension on free surface deformation is neglected. Values of the Weber number (which represents the ratio of the inertial force to surface tension force) are always much greater than unity for all the results presented in this study.
- Thermal effects associated to metal volatilization at the free surface of the bath are ignored.

The complete description of the behaviour of the liquid metal bath combines three models considering:

- the turbulent flow of both the liquid metal and air and the associated heat transfer,
- the distributions of electromagnetic forces (Lorentz forces) in the bath, resulting from the interaction of the current flowing through the metal with both the magnetic field induced by the current and external magnetic field,
- and the dynamic shape of the top surface of the bath.

These three models are fully coupled. For example, the free surface geometry depends on the liquid metal flow, which is governed by Lorentz forces. Reversely, the exact shape of the free surface strongly affects the distribution of Lorentz forces within the bath. The interrelation between the free surface dynamics and the Lorentz forces implies thus to be able to re-calculate the distribution of Lorentz forces after each surface deformation (i.e. at each time step).

Flow modelling

Flow phenomena are described using the Navier-Stokes and energy equations, together with the conservation equations of the turbulent kinetic energy k and the dissipation rate of the turbulent kinetic energy ε. These equations can be written in the general form of a convection-diffusion equation for the variable ϕ, which reads in an axisymmetric cylindrical coordinate system (r, θ, z):

$$\frac{\partial}{\partial t}(\rho\phi)+\frac{1}{r}\frac{\partial}{\partial r}(r\rho u_r\phi)+\frac{\partial}{\partial z}(\rho u_z\phi) = \frac{1}{r}\frac{\partial}{\partial r}\left(r\Gamma_\phi\frac{\partial\phi}{\partial r}\right))+\frac{\partial}{\partial z}\left(\Gamma_\phi\frac{\partial\phi}{\partial z}\right)+S_\phi \quad (1)$$

The expressions of the diffusion coefficient Γ_ϕ and source term S_ϕ are given in Table 1 for each variable of the flow.

μ_{eff} is the effective dynamic viscosity given by $\mu_{\text{eff}}=\mu+\mu_t$, where μ and μ_t are the molecular and turbulent dynamic viscosity. F_r, F_θ and F_z represent the radial, azimuthal and axial components of the Lorentz force in the liquid metal. In the transport equation of axial momentum, the Boussinesq approximation is adopted to express the density ρ in the gravity force, where g is the gravity, ρ_0 the reference density, T_0 the reference temperature and β_{th} the coefficient of thermal expansion. The parameter α_T is given by $\alpha_T=c_p\mu_{\text{eff}}/\lambda_{\text{eff}}$, where $\lambda_{\text{eff}}=\lambda+\lambda_t$ is the effective thermal conductivity and c_p the specific heat.

The k–ε RNG turbulence model is used in this study. This model is a variation of the standard k–ε model, which has been derived using a rigorous mathematical technique called "ReNormalisation Group Theory". It enables in particular more accurate representation of rapidly strained flows and swirling flows [13], which justifies its choice for the present study.

The values of k and ε are used to define the turbulent viscosity:

$$\mu_t=C_\mu\rho\frac{k^2}{\varepsilon} \quad (9)$$

In the case of a swirling flow, the k–ε RNG model corrects the value of viscosity given by Eq. 9, by means of

Table 1 Expressions of the diffusion coefficient Γ_ϕ and source term S_ϕ in Eq. 1 for the different variables ϕ

	ϕ	Γ_ϕ	S_ϕ
Continuity (2)	1	0	0
Conservation of radial momentum (3)	u_r	μ_{eff}	$-\frac{\partial P}{\partial r}+\frac{\partial}{\partial z}\left(\mu_{\text{eff}}\frac{\partial u_z}{\partial r}\right)+\frac{1}{r}\frac{\partial}{\partial r}\left(r\mu_{\text{eff}}\frac{\partial u_r}{\partial r}\right)-2\mu_{\text{eff}}\frac{u_r}{r^2}+\rho\frac{u_\theta^2}{r}+F_r$
Conservation of axial momentum (4)	u_z	μ_{eff}	$-\frac{\partial P}{\partial z}+\frac{\partial}{\partial z}\left(\mu_{\text{eff}}\frac{\partial u_z}{\partial z}\right)+\frac{1}{r}\frac{\partial}{\partial r}\left(r\mu_{\text{eff}}\frac{\partial u_r}{\partial z}\right)+\rho_0 g(1-\beta_{\text{th}}(T-T_0))+F_z$
Conservation of azimuthal momentum (5)	u_θ	μ_{eff}	$-\frac{u_\theta}{r^2}\frac{\partial}{\partial r}(r\mu_{\text{eff}})-\rho\frac{u_r u_\theta}{r}+F_\theta$
Conservation energy (6)	T	$\mu_{\text{eff}}/\alpha_T$	S_T
Conservation of k (7)	k	$\mu_{\text{eff}}/\alpha_k$	$G_k+G_b-\rho\varepsilon$
Conservation of ε (8)	ε	$\mu_{\text{eff}}/\alpha_\varepsilon$	$C_{1\varepsilon}\frac{\varepsilon}{k}(G_k+C_{3\varepsilon}G_b)-C_{2\varepsilon}\rho\frac{\varepsilon^2}{k}-R_\varepsilon$

a weighting function of the form $f(\Omega, k/\varepsilon)$, where Ω is the fluid angular velocity.

The terms G_k and G_b representing the production of turbulent kinetic energy due to, respectively, the mean velocity gradients and buoyancy write as follows:

$$G_k = \mu_{eff}\left[\left(\frac{\partial u_z}{\partial z}\right)^2 + \left(\frac{\partial u_r}{\partial r}\right)^2 + \left(\frac{u_r}{r}\right)^2 + \frac{1}{2}\left(\frac{\partial u_z}{\partial r} + \frac{\partial u_r}{\partial z}\right)^2\right] \tag{10}$$

$$G_b = \beta_{th} g \frac{\mu_t}{Pr_T}\frac{\partial T}{\partial z} \tag{11}$$

The main modification with respect to the standard k–ε model, except the correction of the turbulent viscosity, is the presence of an additional term R_ε in the transport equation of the dissipation rate ε (8):

$$R_\varepsilon = \frac{C_\mu \rho \eta^3 (1 - \eta/\eta_0)}{1 + \beta\eta^3}\frac{\varepsilon^2}{k} \tag{12}$$

where $\eta = S(k/\varepsilon)$ (S is the modulus of the mean rate of strain tensor), $\eta_0 = 4.38$, $\beta = 0.012$.

All the above-defined constants of the turbulence model (C_μ, $C_{1\varepsilon}$, $C_{2\varepsilon}$, $C_{3\varepsilon}$, Pr_T, α_T, α_k, α_ε) are taken equal to the recommended values in the user guide of the Fluent code [13].

Calculation of electromagnetic forces

The Lorentz forces in the liquid metal are defined by the following equations:

$$\vec{F} = \vec{J} \times \vec{B} \tag{13}$$

where $\vec{J}$ is the current density and $\vec{B}$ is the magnetic field, which can be decomposed into an azimuthal component B_θ corresponding to the self-magnetic field induced by the current and an axial component $B_{ext,z}$ corresponding to the magnetic field produced by the external coil around the crucible.

In cylindrical coordinates, the three components of the Lorentz force are given by:

$$F_r = -J_z B_\theta \tag{14}$$

$$F_\theta = J_r B_{ext,z} \tag{15}$$

$$F_z = J_r B_\theta \tag{16}$$

Thus, the self-magnetic field B_θ causes a recirculating flow in the (r,z) plane, whereas the external magnetic field $B_{ext,z}$ gives rise to a circular motion of the metal (azimuthal direction). Note that the circular motion of the metal contributes also to the radial movement through the centrifugal force (term $\rho u_\theta^2/r$ in Eq. 3).

The current density is calculated using the conservation equation of current and the simplified form of Ohm's law, which are given by:

$$\nabla \cdot \vec{J} = S_J \tag{17}$$

$$\vec{J} = \sigma\vec{E} \tag{18}$$

where σ is the electrical conductivity, $\vec{E}$ is the electric field and S_J is a volume source term which is employed, as will be presented below, to implement the boundary conditions on the free surface of the melt.

In Eq. 18, we have ignored the additional current density induced by the motion of the molten metal across the magnetic field lines (i.e. term $\sigma(\vec{u} \times \vec{B})$) compared to the imposed current density. This approximation is supported by the estimates of the ratio of the induced current density associated with $\vec{B}_{ext}$ to the imposed current density, as well as the ratio of the induced current density associated with $\vec{B}_\theta$ to the imposed current density.

The ratio of the induced current density associated with $\vec{B}_{ext}$ to the imposed current density may be scaled as:

$$\frac{\left|\sigma(\vec{U} \times \vec{B}_{ext})\right|}{\left|\sigma\vec{E}\right|} \approx \frac{\sigma U B_{ext} R^2}{I} \tag{18a}$$

As a first approximation, an order of magnitude of the velocity U may be estimated by considering that the convective and electromagnetic terms in the Navier-Stokes equation balance each other:

$$U \approx \sqrt{\frac{IB_{ext}}{\rho R}} \tag{18b}$$

In view of relation (18b), we can rewrite expression (18a) as follows:

$$\frac{\left|\sigma(\vec{U} \times \vec{B}_{ext})\right|}{\left|\sigma\vec{E}\right|} \approx \frac{\sigma B_{ext}^2 R}{\rho U} = \frac{Ha^2}{Re} \tag{18c}$$

Here, $Ha = B_{ext}R\sqrt{\sigma/\rho\nu}$ and $Re = UR/\nu$ are the Hartmann and Reynolds numbers, respectively. Note that the ratio Ha^2/Re is also known as the Stuart number or interaction parameter in the MHD literature.

For the conditions investigated in this study ($R = 0.15$ m, $I = 8$ kA, $B_{ext} \sim$ 2–9 mT), the ratio $Ha^2/Re(= \sigma B_{ext}^{1.5} R^{1.5}/\rho^{0.5} I^{0.5})$ remains small compared to unity (typical values are 7.10^{-4}–7.10^{-3}). Therefore, the induced current density associated with $\vec{B}_{ext}$ can be neglected. Note that this conclusion may be additionally verified by directly evaluating expression (18a) (without inclusion of approximation (18b)) a posteriori from the simulation results, which yields values of 2.10^{-3}–2.10^{-2}.

Following the same approach, it can be demonstrated that the induced current density associated with $\vec{B}_\theta$ is more than two orders of magnitude smaller than the imposed current density (the ratio Ha^2/Re is of the order of 9.10^{-3} in that case) and can therefore also be ignored in Eq. 18.

Combining Eqs. 17 and 18, we derive a differential equation for the electrical potential (defined by $\vec{E} = -\nabla\phi$):

$$\nabla \cdot (\sigma \nabla \phi) = S_J \tag{19}$$

The solution of this equation (in the liquid metal region only) yields the distribution of the electrical potential, from which the current density can be obtained using Ohm's law (18).

The azimuthal magnetic field B_θ is calculated using Ampere's law:

$$B_\theta = \frac{\mu_0}{r} \int_0^r J_z r \, \mathrm{d}r \tag{20}$$

where μ_0 is the magnetic permeability of vacuum.

Calculation of the free surface deformation

The method used to represent the shape and to track the motion of the free surface is the well-known Volume Of Fluid (VOF) technique. In this method (pioneered by Hirt and Nichols [14] and further improved by numerous authors), the free surface location is represented implicitly by means of a variable F associated to each computational cell, which represents the volume fraction of the liquid metal in the cell. The values of the variable F are as follows:

$F = 1$	in cells full of liquid metal
$F = 0$	in cells full of air
$0 < F < 1$	when a cell contains the free surface

In order to track the movement of the free surface throughout the domain, the following transport equation is solved:

$$\frac{\partial F}{\partial t} + \frac{1}{r}\frac{\partial}{\partial r}(r u_r F) + \frac{\partial}{\partial z}(u_z F) = 0 \tag{21}$$

The calculation of the free surface deformation proceeds into two steps. First, the free surface is reconstructed in each interface cell from the distribution of the volume fraction in the surrounding cells. In this step, the piecewise-linear interface calculation (PLIC) method of Youngs [15], as implemented in Fluent, is used. Second, the reconstructed surface is advected based on calculated face fluxes for each fluid. In the computational cell containing the free surface, the physical properties of the fluid mixture (density, viscosity) are expressed as an average of the properties of the mixture components, weighted by the volume fraction of each fluid.

Boundary conditions

Boundary conditions need to be specified at three types of boundaries (see Fig. 2): the top boundary of the computational domain, the crucible wall and the symmetry axis.

On the top boundary, pressure is given and the turbulent kinetic energy and its dissipation rate are arbitrarily fixed to a small value (i.e. $k = 1\ \mathrm{m^2/s^2}$, $\varepsilon = 1\ \mathrm{m^2/s^3}$). On the crucible wall, boundary conditions express cancellation of the velocity. To represent damping of the turbulence very close to the wall, the standard wall functions proposed by Launder and Spalding [16] are used. Wall temperature is uniform and equal to the liquidus temperature of the metal. The electrical potential, uniform as well, is arbitrarily fixed to $\phi = 0$. At the symmetry axis, the radial component of the velocity and the radial gradient of all variables are zero.

Distributions of the current density and temperature at the free surface of the bath

The correct representation of the distributions (considered to be uniform) of the temperature and current density at the free surface of the bath is an essential aspect to achieve a representative simulation of the liquid pool. However, it is a delicate task owing to the moving character of the free surface, whose shape furthermore does not align with any line of the fixed computational grid. Another difficulty is related to the Fluent code framework, which does not permit the modifications of the discretization variables (e.g. fluxes across cell faces).

In this work, the following approximate procedure was used. An additional source term in the energy Eq. 6 (resp. electrical potential Eq. 19) is introduced, which enables to fix the value of the temperature (resp. the current density).

The volume source term employed in the energy equation is defined as (following the notations employed in Table 1):

$$S_T = \frac{K}{c_p}(T_{surf} - T) \tag{22}$$

where T_{surf} is the temperature of the molten metal. The constant K is set to a very large value (typically $10^{12}\ \mathrm{W\ m^{-3}\ K^{-1}}$) to ensure that the source term dominates all other terms of the discretized energy equation.

Regarding the current conservation equation (Eq. 19), we use the following volume source term:

$$S_J = \frac{I}{\pi R_{bath}^2}\frac{A}{V} \tag{23}$$

where I is the total current intensity, R_{bath} is the bath radius, A and V are, respectively, the top face area and the volume of the computational cell.

The source terms are only applied in the cells crossed by the free surface, defined as a first approximation by the iso-value 0.5 of the volume fraction. A more sophisticated approach, involving the application of the source term in a thin transition region representing the free surface or accounting for the local orientation of the free surface in each cell, could be included in a further study.

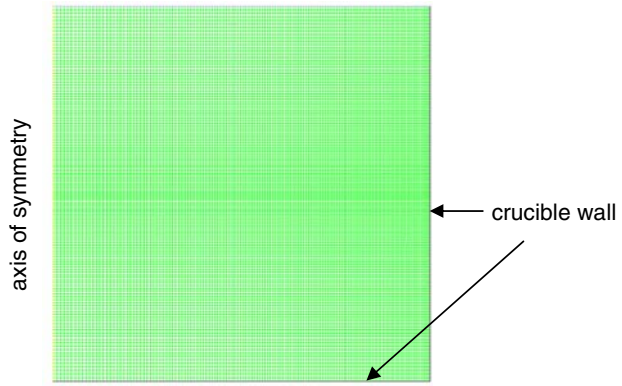

Fig. 3 Computational mesh

Numerical method

The equations relative to the turbulent flow and the free surface deformation are simulated using the code Fluent v6.2.16. A segregated solution algorithm has been used, with the following discretization scheme: first order accurate in time and second order accurate in space. Electromagnetic field calculations are not addressed by the standard version of the Fluent code. To solve Eq. 19 for the electrical potential and calculate the distribution of Lorentz forces inside the metal, we developed a user module consisting of a series of C subroutines (User Defined Function). The grid, refined near the free surface of the bath and the lateral wall of the crucible, consists of 19881 cells (Fig. 3). The size of the smallest cells is equal to 737 μm. The time step is equal to 0.01 s. A typical simulation requires around 8 days of CPU time on a present day PC computer. Study of grid refinement and time step refinement shows that further increase in the grid cell number and time step has essentially no influence on the simulation results.

Model verification

The model predictions have been compared with the results of the code SOLAR dedicated to VAR simulation. For this purpose, SOLAR has been slightly adapted in order to be able to handle the configuration of Fig. 2. In particular, boundary conditions have been modified so as to impose the liquidus temperature at the crucible walls and the melting rate has been set to zero. In contrast to the model developed in this study, the SOLAR code is based on a simplified standard k–ε turbulence model, which does not take into account the production of turbulent kinetic energy due to buoyancy. In order to get rid at least partly of the differences in the description of the turbulence between the two models, the buoyancy forces were cancelled, by carrying out the computation for the case of an isothermal flow at the liquidus temperature. In this section, only the liquid metal region is considered in the calculation and the free surface is assumed to be flat and to remain steady. Calculations have been conducted for a liquid zirconium bath of diameter 0.3 m and height 0.075 m. The current intensity across the bath is equal to 8 kA. The vertical magnetic field density inside the bath is uniform and equal to 4.5 mT. Physical properties of liquid zirconium are shown in Table 2. Note that the melt and stirring parameters chosen in the present paper do not reflect any standard production practice employed by CEZUS.

Table 2 Physical properties of liquid zirconium used in the simulations

Parameter	Value
ρ_0	6240 kg/m^3
c_p	401 J/kg/K
λ	43.5 W/m/K
μ	4.83×10^{-3} kg/m/s
β_{th}	6.10^{-6} K^{-1}
σ	10^6 Ω^{-1}/m

The results described here refer to the stationary regime. The vertical profiles (for a radius $r = 0.126$ m) of the three components of the Lorentz force, obtained with the present model and using SOLAR, are compared in Fig. 4. There is an excellent agreement between the two models. As illustrated in Fig. 5, the velocity vector fields predicted by Fluent and SOLAR are very close. The flow consists of an important recirculating loop along the crucible lateral wall, which results from the combined effects of the Lorentz and centrifugal forces. The difference between the maximal values of the velocity predicted by Fluent and SOLAR (0.6 and 0.51 m/s, respectively) is of the order of 15%. Figure 6 compares the vertical profiles (again for a radius $r = 0.126$ m) of the three components of velocity presently calculated with the predictions by SOLAR. Again, the two models agree rather well. The observed discrepancies are likely to be due to the differences between the two versions of the k–ε model. It is concluded from the results of this comparative study that the developed model provides a satisfactory representation of the behaviour of the liquid pool during a VAR operation.

Results and discussion

Simulations have been performed for the same melt parameters as those employed in section "Model Verification". Initially, the bath is motionless and its surface is perfectly horizontal. Temperature of the free surface of the

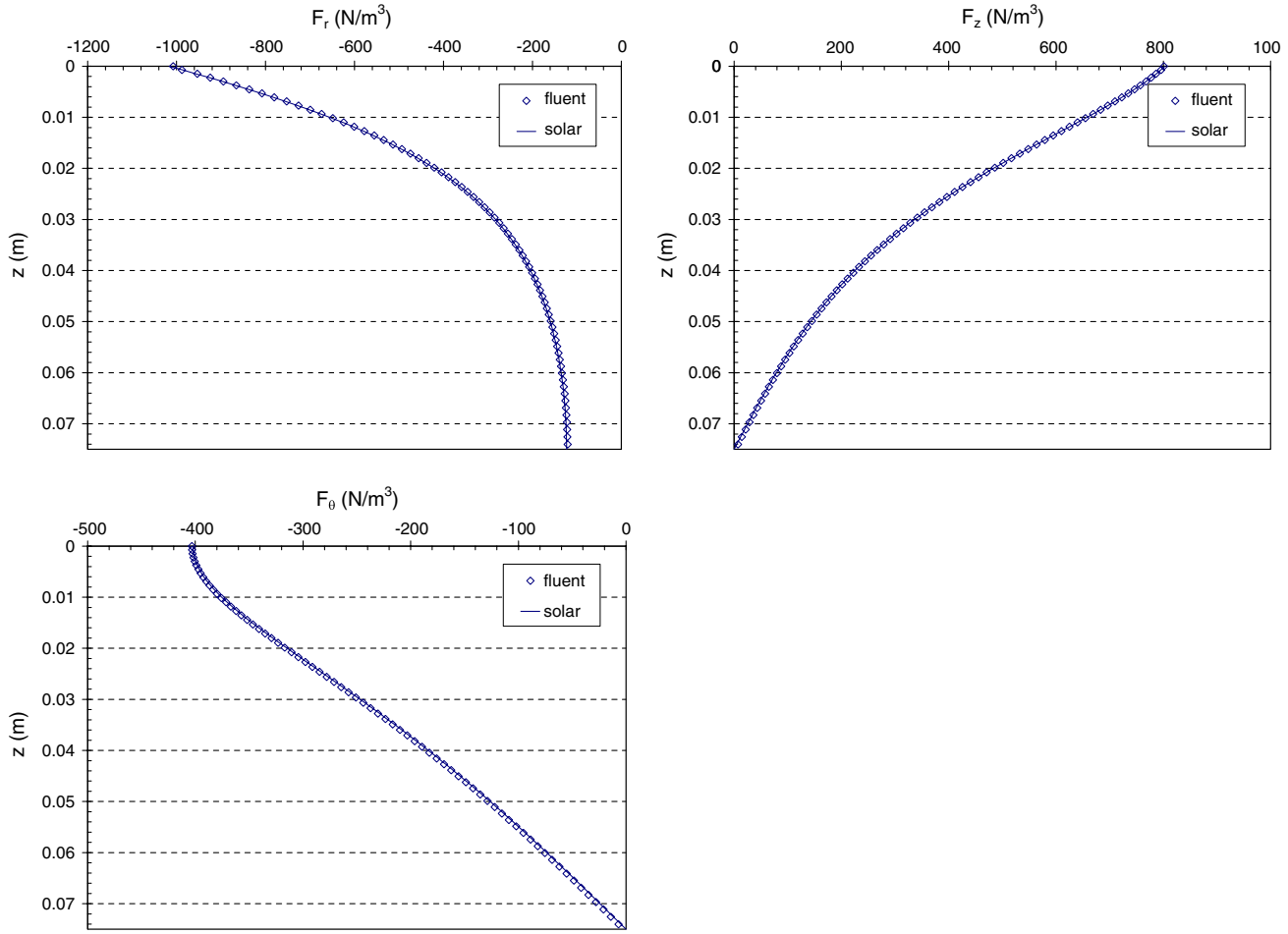

Fig. 4 Comparison of simulated axial profiles of the Lorentz force components F_r, F_z and F_θ at $r = 0.126$ m with those predicted using the SOLAR code

bath is equal to 2000 K. Two modes of stirring (unidirectional and alternated), especially designed for the purpose of the present study, have been considered in the calculations. They are represented schematically in Fig. 7.

General effect of electromagnetic stirring on the free surface deformation

Unidirectional stirring

In this subsection, the magnetic field density is constant and equal to 4.5 mT. The shape of the free surface calculated at different time instants is presented in Fig. 8. The Lorentz force produced by the external magnetic field induces an azimuthal movement of the metal in the bath. Under the effect of the centrifugal force associated to this azimuthal movement, the free surface is progressively depressed, until it reaches a characteristic equilibrium shape in the form of a concave dome. The equilibrium shape of the surface is governed by a balance between the Lorentz forces, hydrodynamic pressure and gravity. Note that the transition to a stationary shape of the free surface is relatively long (about 80 s), due to inertial effects. The steady state amplitude of the surface deformation (i.e. the height difference between the contact point of the surface with the crucible wall and the level of the metal at the centre of the bath) is equal to 2.54 cm (Fig. 9).

The high frequency and small amplitude oscillations of the surface deformation amplitude observed in Fig. 9 are a numerical noise associated to the discretization scheme of the transport equation of the volume fraction (21). In the early stages of the transient regime, the deformation amplitude takes negative value. Such a behaviour is due to the particular instantaneous structure on the flow in the bath. These results are naturally affected by the description of the contact between the metal and the crucible wall. The model presented in this study could be improved in the future by taking into account the contact angle of the metal with the wall.

Figure 10a shows the velocity vector field in the bath for the stationary regime. The flow consists of two main

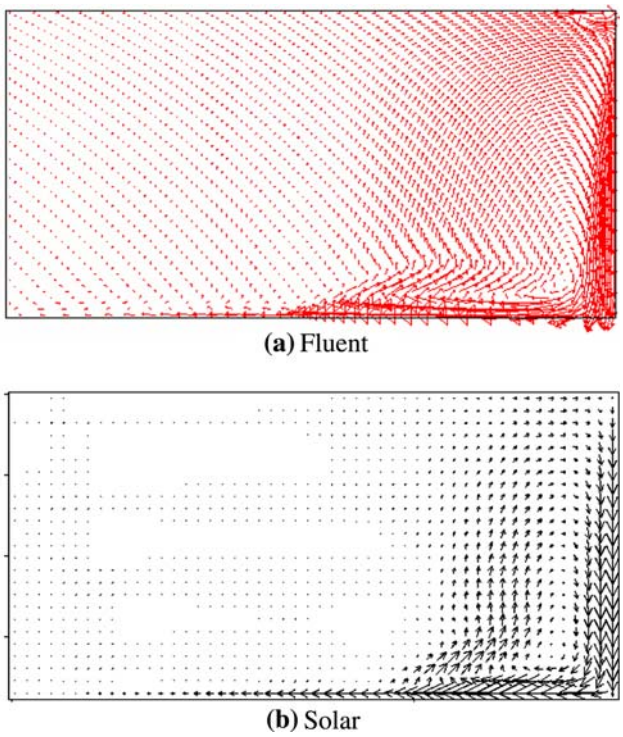

Fig. 5 Flow fields of the liquid metal in the bath obtained (**a**) by the present model and (**b**) by the code SOLAR

recirculating loop of opposite direction: one (clockwise) along the lateral wall surface and the other (anti-clockwise) near the meniscus. The simulation accounting for the deformation of the free surface provides a velocity field markedly different than a simulation assuming a fixed and flat surface (Fig. 10b). Thus, the assumption which consists in neglecting the movements of the free surface may lead to serious errors, not only regarding the shape of the free surface, but also regarding the prediction of the velocity field (in particular near the top).

Figure 11 shows the contours of the turbulent to molecular viscosity ratio in the bath at 90 s (i.e. in the steady state), as an illustration of the turbulence level. A moderate level of turbulence is observed in the whole bath, with a maximal value of the ratio of approximately 110. As it could be expected, the highest levels of turbulence occur in the vicinity of the lateral wall, where the swirl flow is the most intense.

Alternated stirring

The results presented in this subsection refer to the alternated stirring mode, with a magnetic field density of 4.5 mT and a reversal time of the magnetic field T equal to 60 s. In the case of alternated stirring, the dynamics of the free surface is much more complex than during unidirectional stirring. Figure 12 shows the transient evolution of the surface deformation at the centre of the bath and at the crucible wall. The transient evolution of the amplitude of the free surface deformation is presented in Fig. 13. The deformation follows, after a 60 s transient regime, a periodic evolution of period T, which is governed by the magnetic field reversal. Note that the appearance of a period equal to T is natural. Indeed, it can be readily anticipated that the two rotation directions (clockwise and anti-clockwise) of the metal have the same effect on the deformation of the free surface.

During the first part of a reversal period ($0 < t < T/4$), the deformations at the centre of the bath and at the crucible wall decrease rapidly, whereas the second part of a reversal period ($T/4 < t < T$) is characterized by an increase of the deformations. The amplitude of deformation reaches its maximum value (about 2.27 cm in the present case) when the magnetic field is reversed. It can be seen that during some time interval around the time instant associated to the change in the direction of variation of the deformations, the amplitude of deformation is negative (metal level is higher at the centre of the bath than near the crucible wall). This is due, like in unidirectional stirring, to the particular transient structure of the flow.

Figure 14 shows the dynamics of the free surface during a reversal period. The reversal of the magnetic field seriously disturbs the free surface geometry, especially in the early stages following the reversal. It appears a system of concentric waves of small amplitudes that propagate over all the surface of the bath. During the second part of the reversal period, the surface waves are totally damped and the free surface has a concave dome shape. In this example, the free surface does not reach an equilibrium shape during a reversal period.

Influence of the magnetic induction and reversal time

The effect of the magnetic induction on the maximum amplitude of the deformation of the free surface is illustrated in Fig. 15 in the case of unidirectional stirring. As expected, the amplitude increases with the magnetic induction. In the range of induction values considered here, the amplitude increase is linear (with a linear regression coefficient of the order of 6.9 m/T). A 100% variation of the magnetic induction yields an increase of about 260 % of the deformation amplitude.

In Fig. 16, the maximum deformation amplitude of the free surface in alternated stirring is represented for different values of the reversal time (for a fixed magnetic induction of 4.5 mT). Obviously, the deformation amplitude is more important when the period increases. In the case of short periods (<30 s), the free surface is moderately affected by the stirring and the maximum amplitudes remains relatively small (<1 cm). For periods longer than

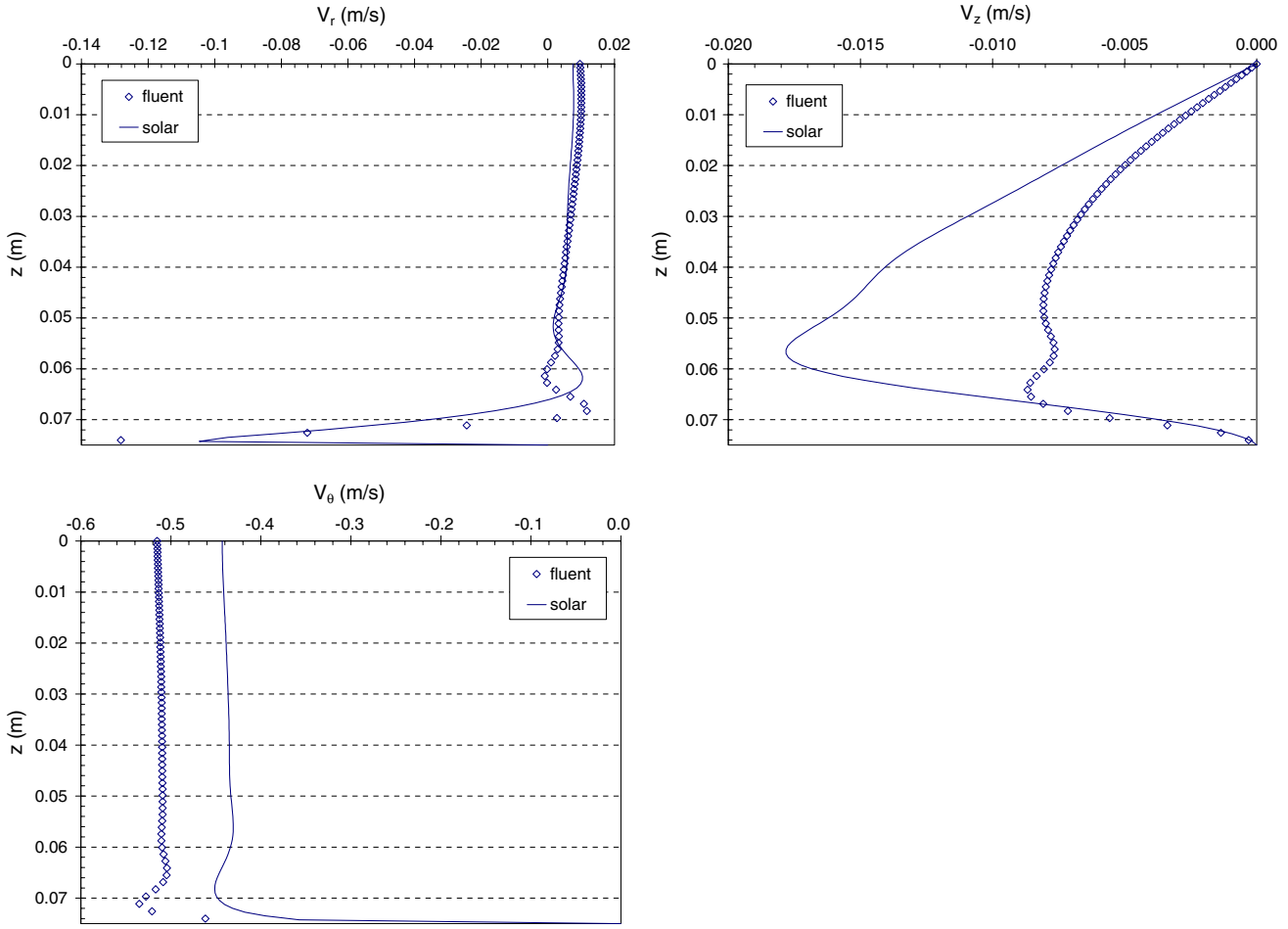

Fig. 6 Comparison of simulated axial profiles of the velocity components v_r, v_z and v_θ at $r = 0.126$ m with those predicted using the SOLAR code

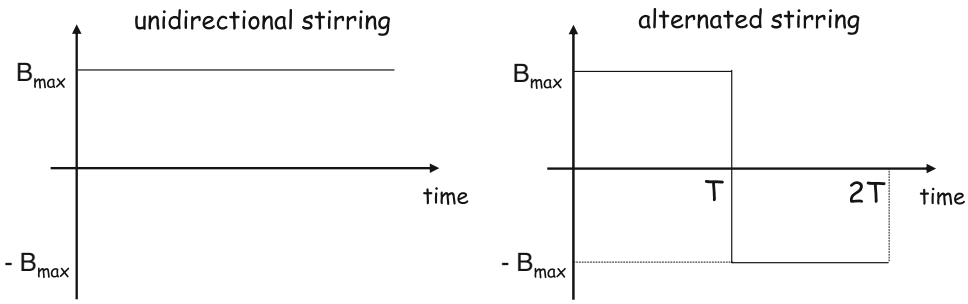

Fig. 7 Schematic diagram of the unidirectional and alternated stirring mode of the liquid metal bath

120 s, there appears an asymptotical regime, corresponding to a maximum deformation amplitude identical to the stationary amplitude obtained under unidirectional stirring (Fig. 9).

Application to the VAR process: influence of free surface deformation on ingot skin

In this subsection, we simulate the dynamics of the pool free surface, taking into account in a simplified way the ingot growth inside the crucible, resulting from the continuous supply of liquid metal from the melting of the consumable electrode.

Figure 17 shows the typical temporal evolution of the liquid metal level at the crucible wall (i.e. height of the contact point of the pool free surface with the crucible wall) under the combined effect of the ingot growth and the surface deformation induced by alternated electromagnetic stirring. The calculations have been conducted for different constant values of the melt rate of the consumable

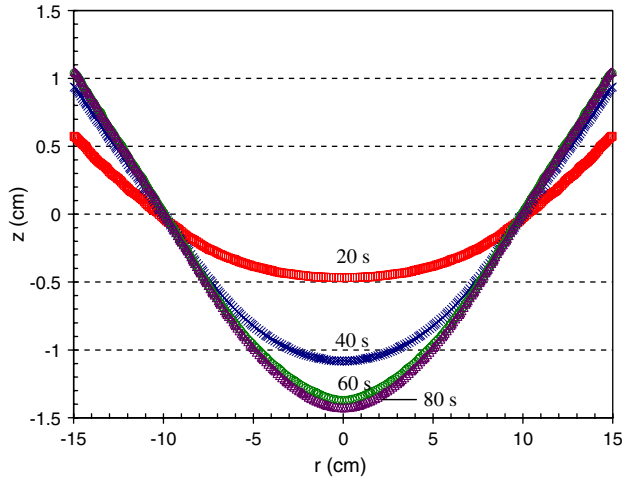

Fig. 8 Computed transient evolution of the free surface shape under unidirectional stirring (magnetic induction of 4.5 mT)

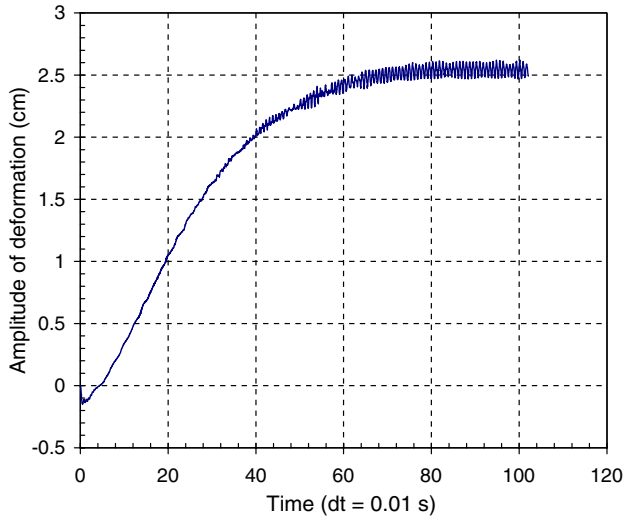

Fig. 9 Computed transient evolution of the amplitude of the free surface deformation under unidirectional stirring (magnetic induction of 4.5 mT)

electrode (i.e. ingot growth rate), a magnetic induction of 4.5 mT and reversal time of 60 s. Note that if we assume the surface undeformable and the growth rate constant, the liquid metal level increases linearly inside the crucible. When the surface is free to deform, one observes an upward velocity of the liquid metal level significantly irregular, in response to the free surface fluctuations induced by the electromagnetic stirring. In particular, it is seen that the metal levels move down the crucible periodically (after each reversal of the magnetic field), which results from the fact that the supply of metal at the top of the bath is not sufficient to compensate for the deformation of the surface. The smaller the ingot growth rate, the more important this effect.

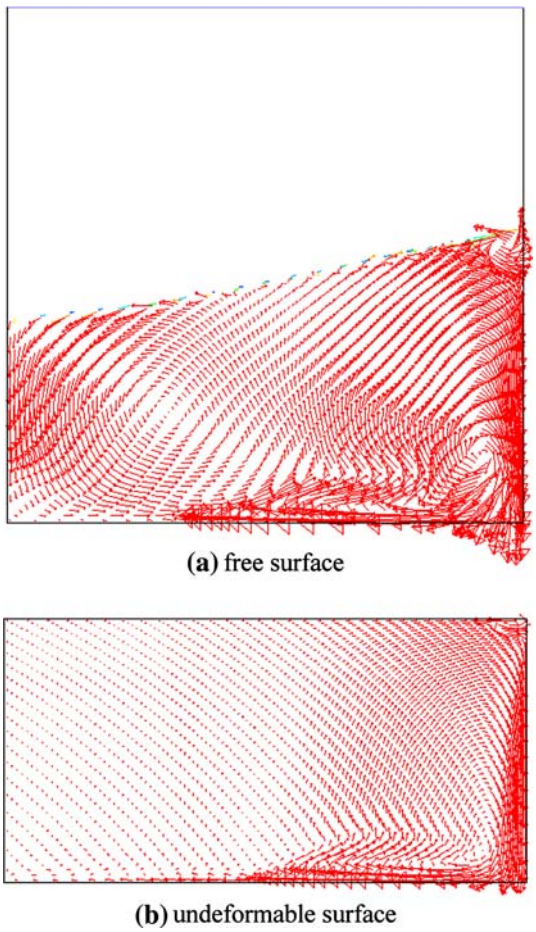

Fig. 10 Flow fields of the liquid metal in the bath under unidirectional stirring obtained at steady state when (**a**) taking into account and (**b**) ignoring the deformation of the free surface

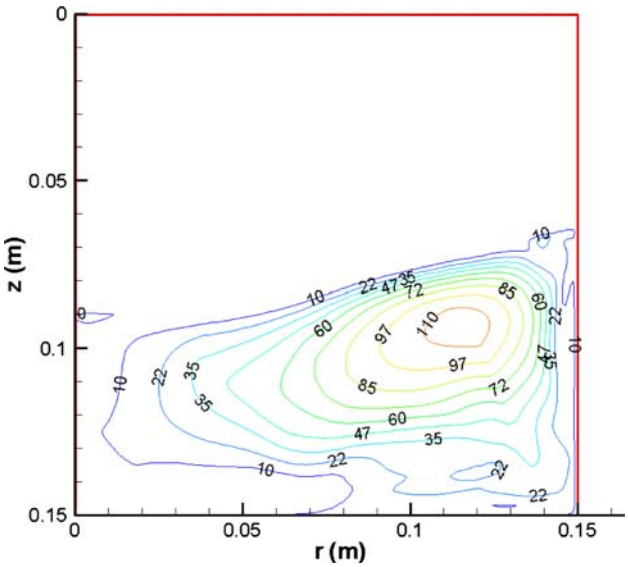

Fig. 11 Computed contours of the turbulent to molecular viscosity ratio in the metal bath at steady state (magnetic induction of 4.5 mT)

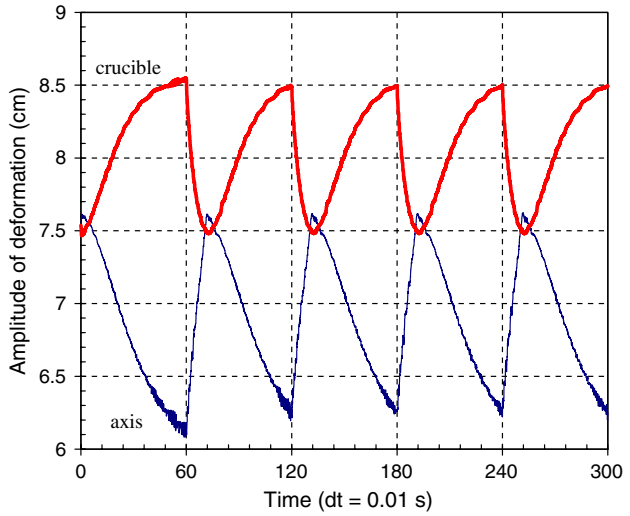

Fig. 12 Computed transient evolution of the free surface deformations at the centre of the bath and at the crucible wall under alternated stirring (reversal time of 60 s)

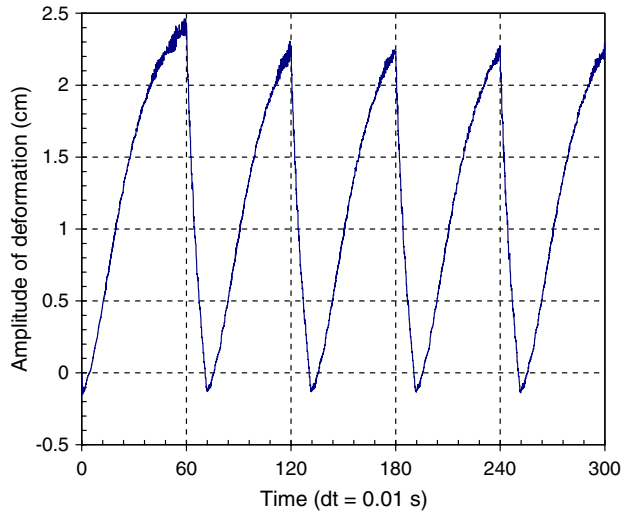

Fig. 13 Computed transient evolution of the amplitude of the free surface deformation under alternated stirring (reversal time of 60 s)

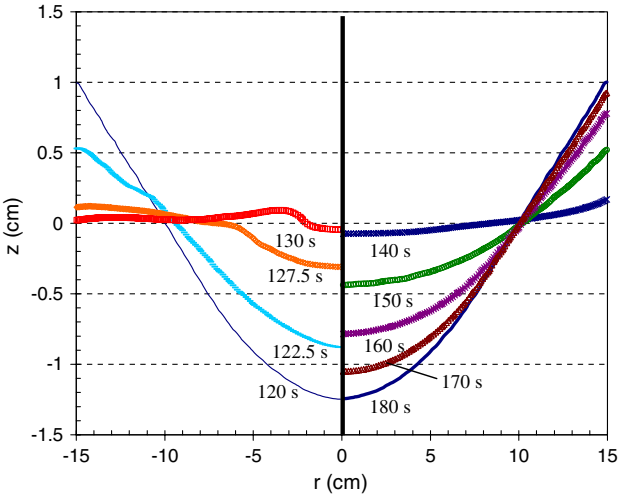

Fig. 14 Computed transient evolution of the free surface shape during a reversal period

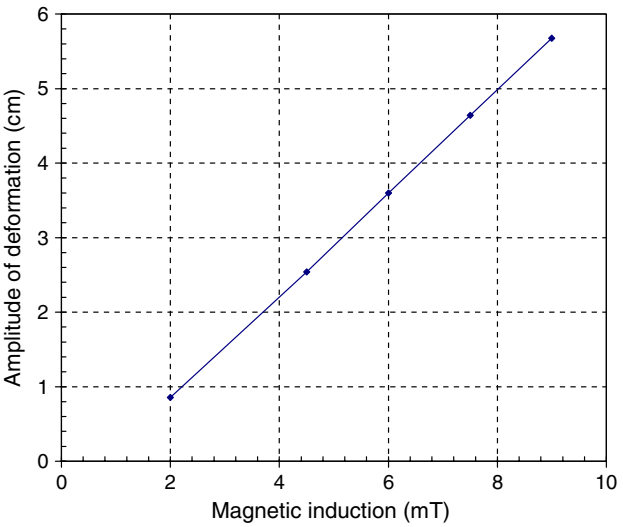

Fig. 15 Influence of the magnetic induction on the maximum amplitude of the free surface deformation under unidirectional stirring

The main effect of the ingot growth on the free surface dynamics is to reduce the "effective" amplitude of the fluctuations of the surface (i.e. amplitude of the transient downward motion of the liquid level at the crucible wall). For the range of growth rates investigated in Fig. 17, this effect is relatively important. The "effective" amplitude is indeed of the order of a few millimetres, which is appreciably smaller compared to the value obtained without taking into account the ingot growth (about 1 cm, cf. Fig. 12). The larger the ingot growth rate, the smaller the "effective" amplitude. Note however that the largest value of the growth rate considered here (20 kg/mn) is not sufficient to completely cancel the transient descending movement of the metal level. The results presented in Figs. 15 and 16 have shown that an increase in the magnetic field density and/or in the reversal time lead to an increase of the fluctuation amplitude of the surface. Therefore it may be anticipated that, for a given growth rate, the effect of the ingot growth on the free surface dynamics will be weaker as the magnetic field density and/or in the reversal time increase.

In the VAR process, such fluctuations of the liquid metal level during ingot growth may have an important influence on the solidification conditions of the first solid skin of the ingot in contact with the crucible, hence on the quality of the ingot surface. The fluctuations of the upward velocity of the liquid metal level have a similar effect to that of fluctuations of the melt rate and may be responsible for a significant variation of the thickness of the first solid skin.

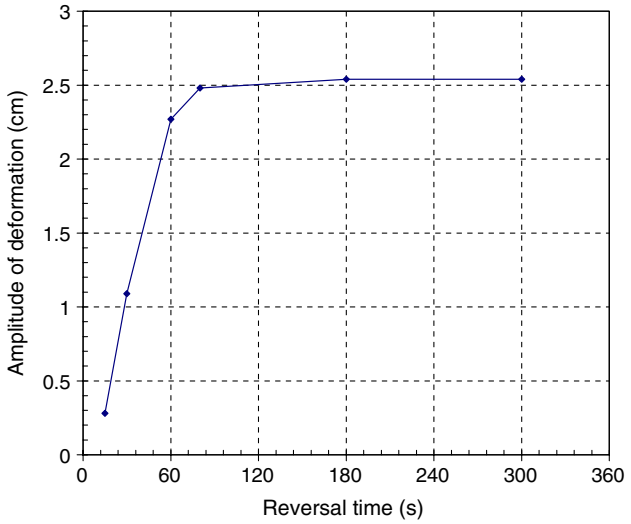

Fig. 16 Influence of the reversal time on the maximum amplitude of the free surface deformation under alternated stirring (magnetic induction of 4.5 mT)

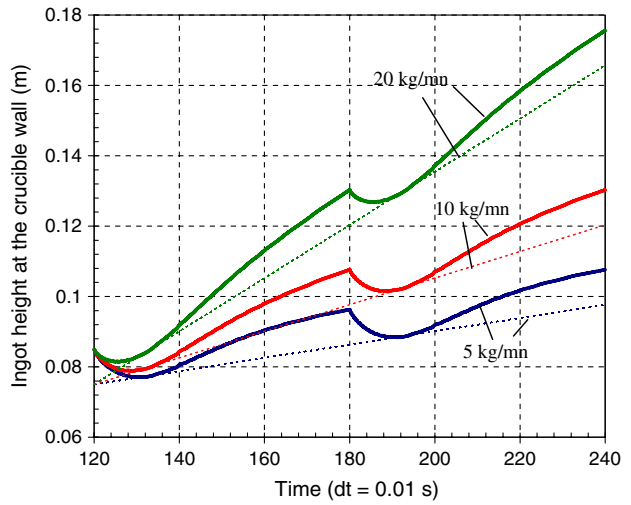

Fig. 17 Computed transient evolution of the ingot height at the crucible wall for different values of the melting rate of the consumable electrode (dashed line: free surface undeformable, full line: surface free to deform)

The periodic downward and upward motion of the liquid level inside the crucible implies the exposition to vacuum and then the covering by fresh liquid metal of a fraction of the solid skin. Depending on the skin thickness, the skin will not be fully remelted during the upward motion of the liquid metal, which may lead to the formation of a new solid skin above the previous one. This phenomenon is most likely to have a negative influence on the ingot surface quality, by contributing to the formation of a so-called "double-skin" (as commonly observed by the process operators). Furthermore, similarly to the observations mentioned in section "Introduction" for the case of the continuous casting process, the first skin may undergo important thermal stresses during metal level fluctuations, which may be responsible for apparition of surface defects (distortion, surface depression, cracks). Thus, the fluctuations of the liquid metal level may affect negatively the surface quality of the remelted ingot.

Conclusions

The deformation of the free surface of a liquid zirconium bath, caused by electromagnetic stirring, has been evaluated quantitatively. The model developed describes the turbulent liquid metal flow and heat transfer and accounts for the coupling between the Lorentz force distribution inside the metal and deformation of the free surface of the bath. A specific procedure has been implemented to take into account the thermal and electrical boundary conditions at the surface.

The accuracy of the model representation of the behaviour of the liquid pool of a VAR ingot was confirmed by comparison with the results obtained using the dedicated code SOLAR. Numerical simulations of the dynamics of the free surface were carried out for two stirring modes: unidirectional and alternated. Under unidirectional stirring, the free surface takes a concave dome shape of relatively small height in comparison to the bath radius. It was shown that the amplitude of deformation is proportional to the magnetic induction for the investigated conditions. Alternated stirring causes periodic fluctuations of the liquid metal level in the crucible, which gives rise to a system of concentric surface waves after each reversal of the magnetic field. The amplitude of deformation remains relatively small for short reversal time (<60 s in this study).

Using the model to study the influence of free surface deformation on the surface quality of a VAR ingot, we have shown that the contact point of the free surface with the crucible wall undergoes oscillatory movement during the ingot growth. This phenomenon, which may contribute to the formation of a "double skin" of the ingot in contact with the crucible, clearly demonstrates (at least qualitatively) the potentially negative influence of the fluctuations of the liquid metal level on the ingot surface quality. Experimental observations would be naturally necessary to confirm such a conclusion.

Further improvements of the present model can be made by integrating the following to the description of free surface deformation near the crucible wall: surface tension effects and contact angle between the liquid metal and the wall. In order to improve the representativity of the model, it would be necessary to take into account the absence of electrical contact between the metal and the crucible in the

shrinkage region of the VAR ingot, which determines the distribution of the Lorentz force in the bath. Finally, a more detailed (and quantitative) understanding of the impact of the dynamics of the free surface on the ingot surface quality would require to account for solidification phenomena of the ingot skin and the thermo-mechanical behaviour of the skin.

References

1. Davidson PA, He X, Lowe AJ (2000) Mater Sci Tech 16:699
2. Xu X, Zhang W, Lee PD (2002) Metall Mater Trans A Phys Metall Mater Sci 33:1805. doi:10.1007/s11661-002-0189-z
3. Quatravaux T, Ryberon S, Hans S, Jardy A, Lusson B, Richy PE et al (2004) J Mater Sci 39:7183. doi:10.1023/B:JMSC.0000048730.26836.68
4. Mitchell A (2005) Mater Sci Eng A 413–414:10. doi:10.1016/j.msea.2005.08.157
5. Hans S, Jardy A, Ablitzer D (1994) In: Mitchell A, J. Fernihough J (eds) Proceedings of international symposium on liquid metal processing and casting, Santa Fe, USA, p 143
6. Wilson AF, Hamel J, Fox SP, Jardy A, Ablitzer D (2003) In: Proceedings of the 10th world conference on titanium, Hambourg, Germany
7. Thomas BG, Zhu H (1995) In: Ohnaka I, Stefanescu D (eds) Proceedings of international symposia on advanced materials & tech. for 21st century, Honolulu (USA), TMS, Warrendale, PA, p 197
8. Kumar S, Meech JA, Samarasekera IV, Brimacombe JK, Rakocevic V (1999) Ironmak Steelmak 26:269. doi:10.1179/030192399677130
9. Thomas BG, Jenkins MS, Mahapatra RB (2004) Ironmak Steelmak 31:485. doi:10.1179/030192304225019261
10. Yasunaka H, Taniguchi K, Kokita M, Inoue T (1995) ISIJ Int 35:784. doi:10.2355/isijinternational.35.784
11. Bocher G, Obermann R, Winklre B, Kruger G, Patte P (1991) In: Proceeding of 1st European Conference on Continuous Casting, Florence, Associazione Italiana di Metallurgica, Milan, Italy, p 205
12. Hans S (1995) Modélisation des transferts couples de chaleur, de soluté et de quantité de mouvement lors de la refusion à l'arc sous vide (VAR)—Application aux alliages de titane, Thèse INPL (in french)
13. Documentation FLUENT (User's Guide, UDF Manual) Version 6.2.16, Fluent, Inc., Lebanon, New Hampshire (2005)
14. Hirt CW, Nichols BD (1981) J Comput Phys 39:201. doi:10.1016/0021-9991(81)90145-5
15. Youngs DL (1982) In: Morton KW, Baines MJ (eds) Numerical methods for fluid dynamics. Academic Press, New York, p 273
16. Launder BE, Spalding DB (1974) Comput Methods Appl Mech Eng 2:269. doi:10.1016/0045-7825(74)90029-2